Proceedings of the 17th World Congress
The International Federation of Automatic Control
Seoul, Korea, July 6-11, 2008

Glidepath Command Generation and Tracking for Longitudinal Autolanding

Hann-Shing Ju Ching-Chin Tsai*

Electrical Engineering Department, National Chung-Hsing University,
*Taichung, Taiwan, ROC, (*e-mail: cctsai@dragon.nchu.edu.tw)*

Abstract: This paper describes a glidepath command generator for indirect altitude control and presents an auto-landing controller for glide-slope tracking and flare maneuver via adaptive backstepping, in order to provide precise altitude trajectories for auto-landing of unmanned aerial vehicles. The proposed glide-slope tracking and flare maneuver control law is quite different from conventional guidance and control loops separately designed in autopilot. Simulation results demonstrate that the adaptive auto-landing controller is capable of effectively guiding the aircraft along the glidepath command under the presence of the wind disturbances and microburst.

1. INTRODUCTION

The design of auto-landing controller has been considered a very challenging problem. An important part of an autopilot is the control of an aircraft's longitudinal dynamics, and the most puzzling work of longitudinal autopilot is the automatic landing task. Many control researchers have developed several methodologies to achieve auto-landing flight control design, including PID (Ebrahimi and Coleman, 2001; Ha and Kim, 2005; Iiguni and Akiyoshi, 1998), LQR (Kim, *et al.*, 2005), intelligent control (Iiguni and Akiyoshi, 1998), neural networks (Izadi, *et al.*, 2003; Jorgenson and Schley, 1990; Juang and Cheng, 2001; Saini and Balakrishnan, 1997), fuzzy logic (Nho and Agarwal, 2000), and H_∞ synthesis (Kaminer and Khargonekar, 1990; Li, *et al.*, 2004; Niewoehner and Kaminer, 1996; Ochi and Kanai, 1999; Shue and Agarwal, 1999). Some of the designs of auto-landing used classical control techniques; these are the stability augmentation of the inner loop and the path tracking of the outer loop (Kaminer and Khargonekar, 1990; Jorgenson and Schley, 1990; Iiguni and Akiyoshi, 1998). Although these intelligent controllers are relatively simple and easy to implement, most of the controllers lack in guaranteeing stability. Many researchers have successfully derived H_∞ controllers for different classes of aircrafts, whose robust control techniques are considered to deal with the uncertainties in wind turbulence and aerodynamics coefficients. However, a high-gain system will most likely occur and a high-order controller's implementation will be complicated.

All the aforementioned studies assumed that the flight path trajectory for glide-slope and flare mode is predetermined for guiding an aircraft, and these investigations did not put emphasis on studying the flight path trajectories. However, the auto-landing controller for low-cost unmanned aerial vehicles (UAVs) should meet the following criteria: simple and easy implementation, guaranteed stability and performance, a viable candidate for flight test, and easy connection to the flight control of waypoint navigation. To design such a controller, we introduce the glidepath command for mandating a straight approach path. The glidepath command and controller are combined to concurrently produce the desired altitude trajectories for the UAV auto-landing, thereby resulting in a simple and pragmatic auto-landing controller. Recently, the Lyapunov-based design method has been developed for aircraft flight control systems (Harkegard and Torkel, 2000; Lee and Kim, 2001; Sharma and Ward; 2002; Ju and Tsai, 2007). These studies utilized the backstepping method to construct stable nonlinear controllers in order to improve the performance of flight path control systems. This paper extends the previous result in Ju, *et al.* (2005) to propose a glide-slope tracking controller via backstepping. The previous work neither described the flare control nor derived the adaptive rules for the model uncertainties. To overcome these shortcomings, the adaptive longitudinal auto-landing control law is derived using the backstepping method with parameter adaptation, and this type of control structure is a cascaded control with eight parameters.

The objective of the paper lies in recalculating the general and exponential altitude equations to derive a desired flight path trajectory, and using the well-known backstepping design procedure to establish a longitudinal auto-landing control law and achieve the desired glide-slope and flare trajectories for the UAV. The range of a suitable relative altitude and distance between the aircraft and the airport would presume to be known for engaging the auto-landing task. This kind of longitudinal auto-landing control can be thought of as the glidepath tracking from glide-slope to flare mode. The proposed controller can accomplish the landing tasks from glide-slope and flare mode without addition inputs. Such a control law is first developed based on Lyapunov stability theory via backstepping control, and its adaptive version is then established for parameter uncertainties.

The remainder of the paper is outlined as follows. Section II briefly recalls the well-established linearized aircraft dynamics and the wind turbulence model. In Section III, the geometry of glide-slope and flare segment is described, and the command generator is developed for the desired trajectory. The backstepping procedure is used in Section IV to design a glidepath control for the glide-slope tracking and

the flare maneuver. An adaptive auto-landing control is then derived to cope with parameter variations. Section V conducts nonlinear 6-DOF simulations. Section VI concludes the paper.

2. CONTROL ARCHITECTURE AND SYSTEM MODELS

The auto-landing control architecture includes 1) a command generator for desired trajectory; 2) an aircraft dynamics model with elevator surface deflection and thrust setting; 3) a wind model for evaluating landing performance; 4) an adaptive backstepping controller and a speed controller for providing surface deflection command and throttle setting, respectively. The command generator and the adaptive backstepping controller are described in later sections.

2.1 Aircraft Dynamics Model

The aircraft used in the paper is a light-weight, long endurance mission UAV, which is controlled by elevator, aileron, rudder, and throttle. Consider a linear model of the longitudinal motion of the UAV with the elevator surface deflection and the thrust setting. The motion equations of a longitudinal aircraft with the short-period and the phugoid mode are described by

$$\begin{aligned}\dot{u} &= X_u u + X_w w - g\cos(\gamma_0)\theta + X_{\delta_e}\delta_e + X_{\delta_T}\delta_T \\ \dot{w} &= Z_u u + Z_w w + U_0 q - g\sin(\gamma_0)\theta + Z_{\delta_e}\delta_e + Z_{\delta_T}\delta_T \\ \dot{q} &= M_u u + M_w w + M_q q + M_{\delta_e}\delta_e + M_{\delta_T}\delta_T \\ \dot{\theta} &= q\end{aligned} \tag{1}$$

where u is the longitudinal velocity (ft/sec); q is the pitch rate (rad/sec); θ is the pitch angle (rad); w is the vertical velocity (ft/sec); δ_e is the elevator surface deflection (rad); δ_T is the throttle setting (%); U_0 is the aircraft velocity (ft/sec); g is the gravity (ft/sec^2). The parameters X_*, Z_*, and M_* are stability and control derivatives of the UAV flying in a trimmed condition (at altitude of 200 ft and speed of 70 knots).

2.2 Wind Model

Wind turbulence and wind shear are used for evaluating landing performance. Wind turbulence is modelled by a Dryden spectrum. The sharp step change in the vertical axis represents vertical wind shear (microburst). The disturbance equations for the longitudinal wind and the vertical wind can be found in Liao *et al*. (2005). Fig. 1 shows the wind profile including turbulence and microburst. The wind shear is generated at an altitude of 140 ft.

3. GUIDEPATH COMMAND GENERATION

Aircraft landing task is usually divided into glide-slope tracking (approach), flare, touchdown, and after-landing roll. Since the glide-slope mode and the flare mode are two critical phases in an aircraft's auto-landing task, we will design a longitudinal auto-landing controller only for these two phases. In the glide-slope segment, the conventional flight path guidance usually generates an absolute path inclination by direct altitude control, but our approach aims particularly at achieving the path inclination by glidepath control. Theoretically, controlling the flight-path angle is mathematically equivalent to regulating the vertical speed within constant airspeed. Our proposed auto-landing controller will be used to control aircraft from glide-slope to flare maneuver by following the glidepath command. In what follows describes the glidepath generation algorithm for the glide-slope and flare mode.

3.1 Glide-Slope Mode

The glide-slope is a fictitious line that connects the desired touchdown point with the aircraft under a particular angle. Once the aircraft has tracked the glide-slope, the aircraft will be aligned to the runway if no wind drift occurs. When the aircraft is guided into a steady-state descent along the desired glide-slope trajectory to the point of touchdown, then the trajectory tracking is well accomplished based on the steady-state vertical speed. Tracking of the vertical speed can provide the desired auto-landing trajectory in the longitudinal axis. For the glide-slope tracking, the aircraft follows a constant vertical speed that represents the descent of the aircraft. For approach, a single glide-slope angle (σ) trajectory is usually considered and recommended to set –3 degree. Therefore, under constant airspeed, the desired glidepath command for the glide-slope tracking from the geometry of glide-path is defined by

$$\dot{h}_{ref,GS} = -3^\circ/(180/\pi)U_0 + \tan^{-1}[(h - h_{ref})/x]U_0 k \tag{2}$$

where x is the horizontal distance of the aircraft, and h_{ref} is the desired altitude for glide-slope maneuver. The term $\tan^{-1}[(h - h_{ref})/x]U_0 k$ in (1) is an adjusted command for small glide-path deviation, and k is an adjusted factor.

3.2 Flare Mode

The flare mode is a successive process of determining the initiation flare altitude for a proper landing. For the flare maneuver, the aircraft follows an exponential path that changes the descent path to a curved one, and then the aircraft can raise its nose and sink softly on the runway. The desired altitude (reference altitude, h_{ref}) follows an exponential path defined by

$$h_{ref}(t) = h_0\, e^{-t/\tau} \tag{3}$$

where h_0 is the flare initiation height, τ is the time constant of exponential flare altitude and is defined as the time to close on a runway surface, and t is the current time throughout the flare maneuver. Taking the time derivative of (3) yields

$$\dot{h}_{ref} = -h_0/\tau \exp(-t/\tau) \tag{4}$$

The design of auto-landing control laws usually assumes that the airspeed does not change significantly from glide-slope to flare mode. Consequently, the general kinematics equation can be written as

$$\dot{h} = -w + U_0\theta = U_0(-\alpha + \theta) = U_0\gamma \tag{5}$$

where $\alpha = w/U_0$ is used for small angle of attack. For generating the reference glidepath command, if (5) is equivalent to (4) for small flight-path angle, then the desired flight-path angle (γ_{ref}) for the flare maneuver following an exponential flare is easily expressed by

$$\gamma_{ref}(t) = -h_0/(U_0\tau)\exp(-t/\tau) \tag{6}$$

Note that h_0 can be determined in the beginning of the flare mode at $t = 0$. Afterward the flare initiation height turns out

$$h_0 = -U_0\,\tau\,\gamma_{ref}(0) \tag{7}$$

where $\gamma_{ref}(0)$ is the flight-path angle command at the flare initiation; $\gamma_{ref}(0)$ is set to -3° because of the steady-state

descent following the ideal glide-slope angle ($\sigma = -3^\circ$). If τ is known then h_0 will be determined. The arc of circumference of the flare trajectory is dependent on the time constant. Furthermore, τ is assumed constant and mostly solved by airspeed and the ground distance traveled during the flare. The desired value of τ can be obtained by specifying the horizontal distance of the aircraft with respect to the touchdown point from the flare initiation. The flare initiation height is usually selected by iterative evaluations for vertical visibility and landing categories and is a crucial parameter for a good landing. Initiating the flare too high or too low will make the aircraft float over the runway or reach zero altitude faster than estimated. Therefore, both the time to close on a runway (τ) and the flare initiation height (h_0) directly affects the flare maneuver. The precise calculation of h_0 and τ will result in the accuracy of altitude trajectory during the flare mode. Besides, for soft landing, the vertical speed is usually selected as an optimal value of about -1 to -2 ft/sec. In (5), if constant airspeed for the flare is assumed, then controlling the flight-path angle just before touchdown is equivalent to controlling the vertical speed. The flight-path angle command at touchdown can be calculated by combining (6) and (7)

$$\gamma_{ref,TD} = \gamma_{ref}(0)\exp(-t/\tau) \tag{8}$$

During the flare phase, the airspeed (U_0) is assumed constant for small flight-path angle. Then, (8) can be rewritten as

$$\gamma_{ref,TD} = \gamma_{ref}(0)\exp[-(x-x_0)/(U_0\tau)] \tag{9}$$

where x is the horizontal distance of the aircraft. x_0 is the horizontal distance at the starting point of the flare mode and is defined as the flare initiation distance. Hence, the time constant of exponential flare (τ) can be obtained from (9) and is shown as

$$\tau = -(x-x_0)_{\exp}/U_0\left[\ln(\gamma_{ref,TD}/\gamma_{ref}(0))\right]^{-1} \tag{10}$$

where $(x\text{-}x_0)_{\exp}$ is the expected distance between the initiation height and the touchdown point. A prior $\gamma_{ref,TD}$ should be known before determining τ. From the general altitude equation (5), the flight-path angle of touchdown at constant airspeed will be expressed by

$$\gamma_{ref,TD} = \dot{h}_{TD}/U_0 \tag{11}$$

where $\dot{h}_{TD}$ is the vertical speed reaching zero height. For soft landing, $\dot{h}_{TD}$ is set to be –1.5 ft/s at the completed flare maneuver, and then $\gamma_{ref,TD}$ is found. Employing the aforementioned parameters in (7), (10), and (11) for the exponential flare command (4), one can calculate the glidepath command from flare to touchdown precisely.

4. CONTROL LAWS DESIGN

For indirect altitude control, the glidepath and the airspeed are controlled during the glide-slope and flare modes. The proposed auto-landing controller consists of two parts: a forward speed PI controller to maintain a constant airspeed by the throttle control and a backstepping controller to track longitudinal flight path by elevator control.

4.1 Forward Speed PI Control

Detailed descriptions of the conventional PI controller can be found in Jorgensen and Schley, 1990, including airspeed and elevator control. The throttle command to maintain aircraft's airspeed at a constant value is generated by

$$\delta_T = K_T(u_c - u) + K_T w_T \int_0^t (u_c - u)dt \tag{12}$$

So that u approaches the desired incremental velocity u_c, where u_c is set to be zero.

4.2 Backstepping Control Law Design

The backstepping design is used to derive a control law for the longitudinal auto-landing. The autopilot flight control system generates elevator commands from the glidepath commands in (2) and (4). The motion equations for a longitudinal aircraft are described in (1). However, equation (1) is not suitable for designing flight control laws via backstepping. For the correct form of backstepping design (Harkegard and Torkel, 2000; Sharma and Ward, 2002; Ju, *et al*., 2007), the aircraft equations of motion are described under the following assumptions: 1) the velocity is related to the phugoid mode of the aircraft and excepted from the equations of motion, and the controller to maintain a constant airspeed by the throttle control is proposed; 2) the lift force on the elevator surface deflection is intentionally neglected for deriving the controller, because it is much smaller than the moment contribution (Harkegard and Torkel, 2000; Lee and Kim, 2001; Sharma and Ward, 2002). Thus the equations of motion for aircraft without airspeed control and surface deflection on the lift given by (1) can be rewritten as

$$\begin{aligned} \dot{w} &= Z_w w + U_0 q - g\sin(\gamma_0)\theta \\ \dot{q} &= M_w w + M_q q + M_{\delta e}\delta_e, \qquad \dot{\theta} = q \end{aligned} \tag{13}$$

The angle of attack (α) is a primary motion variable rather than a vertical velocity (w). For small angles: $\alpha = w/U_0$, the equations of motion in (13) becomes

$$\dot{\alpha} = Z_\alpha \alpha + q + Z_\theta \theta,\ \dot{\theta} = q,\ \dot{q} = M_\alpha \alpha + M_q q + M_{\delta e}\delta_e \tag{14}$$

where $Z_\alpha = Z_w$, $Z_\theta = -g\sin(\gamma_0)/U_0$, and $M_\alpha = M_u U_0$. Using $\theta = \alpha + \gamma$, $\ddot{h} = U_0\dot{\gamma}$ and $\dot{\gamma} = q - \dot{\alpha}$ gives a new form

$$\ddot{h} = Z_{\alpha'}\dot{h} - Z_{\alpha'}\theta, \dot{\theta} = q, \dot{q} = -M_{\alpha'}\dot{h} + M_\alpha\theta + M_q q + M_{\delta e}\delta_e \tag{15}$$

where $Z_{\alpha'} = U_0 Z_\alpha$, $M_{\alpha'} = M_\alpha/U_0$ and Z_θ can be ignored because of large U_0. For the glidepath tracking, one defines three new state variables as

$$z_1 = \dot{h}_{ref} - \dot{h}, \quad z_2 = \theta_{des} - \theta, \quad z_3 = q_{des} - q \tag{16}$$

The time derivative of z_1 is

$$\dot{z}_1 = Z_\alpha z_1 + Z_{\alpha'}\theta - Z_\alpha \dot{h}_{ref} + \ddot{h}_{ref} \tag{17}$$

Considering θ as a control input for z_1-dynamics, one regards the desired value of θ as the virtual control law of (17). To derive the virtual control law (θ_{des}), one chooses the following Lyapunov function candidate

$$V_1(z_1) = (1/2)(\lambda\chi_1^2 + z_1^2) \tag{18}$$

where λ is a positive constant, and $\chi_1 = \int_0^t z_1(t)dt$. In order for $\dot{V}_1$ to be negative semidefinite, θ can be chosen as

$$\theta_{des} = (Z_{\alpha'})^{-1}(Z_\alpha \dot{h}_{ref} - \ddot{h}_{ref} - \lambda\chi_1 - K_1 z_1) \tag{19}$$

For $\dot{V}_1$ to be negative semidefinite, the following constraints must satisfy

$$K_1 > Z_\alpha \tag{20}$$

According to the desired θ in (19), z_2-equation and z_1-dynamics are obtained by respectively rewriting (16) and (17) as follows

$$z_2 = (Z_\alpha \dot{h}_{ref} - \ddot{h}_{ref} - \lambda\chi_1 - K_1 z_1)/Z_{\alpha'} - \theta \tag{21}$$

$$\dot{z}_1 = \ddot{h}_{ref} - \ddot{h} = -(K_1 - Z_\alpha)z_1 - \lambda\chi_1 \tag{22}$$

Rearranging with (21) yields

$$Z_{\alpha'}\theta - Z_\alpha \dot{h}_{ref} + \ddot{h}_{ref} = -\lambda\chi_1 - K_1 z_1 - Z_{\alpha'} z_2 \tag{23}$$

Updating z_1-dynamics in terms of z_1 and z_2 by (22) yields

$$\dot{z}_1 = -(K_1 - Z_\alpha)z_1 - Z_{\alpha'} z_2 - \lambda\chi_1 \tag{24}$$

Differentiating (24) gives

$$\begin{aligned}\dot{z}_2 &= [-C_2 + C_1(K_1 - Z_\alpha)]z_1 \\ &\quad + K_1 z_2 + C_1\lambda\chi_1 - q + \dddot{h}_{ref}/U_0 - \ddot{\gamma}_{ref}/Z_{\alpha'}\end{aligned} \tag{25}$$

where $C_1 = K_1/Z_{\alpha'}$ and $C_2 = \lambda/Z_{\alpha'}$

For determining the desired q, another Lyapunov function candidate can be chosen as

$$V_2(z_1, z_2) = (1/2)(\lambda\chi_1^2 + z_1^2 + z_2^2) \tag{26}$$

The time derivative of V_2 along the trajectories of the tracking error dynamics defined by (32) and (33) is

$$\begin{aligned}\dot{V}_2 &= -(K_1 - Z_\alpha)z_1^2 + [-Z_{\alpha'} + C_1(K_1 - Z_\alpha) - C_2]z_1 z_2 \\ &\quad + K_1 z_2^2 + (C_1\lambda\chi_1 - q + \dddot{h}_{ref}/U_0 - \dddot{h}_{ref}/Z_{\alpha'})z_2\end{aligned} \tag{27}$$

In view of (27), the term $-Z_{\alpha'} + C_1(K_1 - Z_\alpha) - C_2$ is assumed to be zero for simplifying the desired q control. We select

$$-Z_{\alpha'} + K_4[C_1(K_1 - Z_\alpha) - C_2] = 0 \tag{28}$$

and hence λ can be determined by

$$\lambda = -Z_{\alpha'}^2/K_4 + K_1(K_1 - Z_\alpha) \tag{29}$$

To make the fourth term negative definite in (27), we select the desired q as

$$q_{des} = C_1\lambda\chi_1 + \dddot{h}_{ref}/U_0 - \dddot{h}_{ref}/Z_{\alpha'} + K_2 z_2 \tag{30}$$

For $\dot{V}_2$ to be negative semidefinite, it is required to have the following constraints

$$K_1 - Z_\alpha > 0, \quad K_2 - K_1 > 0 \tag{31}$$

By substituting (30) into (16), we rewrite z_3-equation as

$$z_3 = C_1\lambda\chi_1 + K_2 z_2 + \dddot{h}_{ref}/U_0 - \dddot{h}_{ref}/Z_{\alpha'} - q \tag{32}$$

For updating z_2-dynamics in terms of z_1, z_2, and z_3 by (32), we can rewrite $\dot{z}_2$ as

$$\dot{z}_2 = [-C_2 + C_1(K_1 - Z_\alpha)]z_1 + (K_1 - K_2)z_2 + z_3 \tag{33}$$

Differentiating (32) gives

$$\begin{aligned}\dot{z}_3 &= [C_1\lambda - C_2K_2 + C_1K_2(K_1 - Z_\alpha) - M_{\alpha'}]z_1 \\ &\quad + [K_1K_2 - K_2^2]z_2 + K_2 z_3 \\ &\quad + [M_{\alpha'}\dot{h}_{ref} - M_\alpha\theta - M_q q + \ddot{h}_{ref}/U_0 - \ddot{\ddot{h}}_{ref}/Z_{\alpha'}] - M_{\delta e}\delta_e \\ &= C_{11}z_1 + C_{22}z_2 + C_{33}z_3 + \phi - M_{\delta e}\delta_e\end{aligned} \tag{34}$$

where

$$\begin{aligned}C_{11} &= C_1\lambda - C_2K_2 + C_1K_2(K_1 - Z_\alpha) - M_{\alpha'} \\ C_{22} &= K_1K_2 - K_2^2, \quad C_{33} = K_2 \\ \phi &= M_{\alpha'}\dot{h}_{ref} - M_\alpha\theta - M_q q + \ddot{h}_{ref}/U_0 - \ddot{\ddot{h}}_{ref}/Z_{\alpha'}\end{aligned} \tag{35}$$

Determining the control law, the third Lyapunov function candidate can be chosen as

$$V_3(z_1, z_2, z_3) = (1/2)(\lambda\chi_1^2 + z_1^2 + z_2^2 + z_3^2) \tag{36}$$

The time derivative of V_3 along tracking error dynamics governed by (24), (28), (33), and (34) is

$$\begin{aligned}\dot{V}_3 &= -(K_1 - Z_\alpha)z_1^2 - (K_2 - K_1)z_2^2 + z_2 z_3 \\ &\quad + z_3(C_{11}z_1 + C_{22}z_2 + C_{33}z_3 + \phi - M_{\delta e}\delta_e)\end{aligned} \tag{37}$$

In view of (37), the first and second terms are negative definite as long as $K_1 > Z_\alpha$ and $K_2 > K_1$, respectively. To make other terms negative definite, the control surface deflection can be selected as

$$\delta_e = [C_{11}z_1 + (C_{22} + 1)z_2 + K_3 z_3 + \phi]/M_{\delta e} \tag{38}$$

Substituting (38) into (37) yields

$$\dot{V}_3 = -(K_1 - Z_\alpha)z_1^2 - (K_2 - K_1)z_2^2 - (K_3 - C_{33})z_3^2 \tag{39}$$

which is negative semidefinite if the following constraints hold

$$K_1 - Z_\alpha > 0, \quad K_2 - K_1 > 0, \quad K_3 - K_2 > 0 \tag{40}$$

The cascaded control law can be obtained as

$$\begin{aligned}M_{\delta e}\delta_e &= k_p(\dot{h}_{ref} - \dot{h}) + k_i\chi_1 - k_\theta\theta - k_q q + k_f\dot{h}_{ref} \\ &\quad + k_v\ddot{h}_{ref} + k_a\dddot{h}_{ref} + k_d\ddot{\ddot{h}}_{ref}\end{aligned} \tag{41}$$

where

$$\begin{aligned}k_p &= [C_{11} - C_1(1 + C_{22} + K_2K_3)] \\ k_i &= [-C_2(1 + C_{22} + K_2K_3) + K_3C_1\lambda] \\ k_\theta &= [(1 + C_{22} + K_2K_3) + M_\alpha], \quad k_q = [K_3 + M_q] \\ k_f &= [(1 + C_{22} + K_2K_3)/U_0 + M_{\alpha'}] \\ k_v &= -[(1 + C_{22} + K_2K_3)/Z_{\alpha'} + K_3/U_0] \\ k_a &= [-K_3/Z_{\alpha'} + 1/U_0], \quad k_d = -1/Z_{\alpha'}\end{aligned}$$

4.2 Adaptive Backstepping Control Law Design

In this subsection, the adaptive auto-landing control law is synthesized to compensate for parametric uncertainties. The control law (41) can be rewritten with adjustable parameters $k_p, k_i, k_\theta, k_q, k_f, k_v, k_a$, and k_d as

$$\begin{aligned}M_{\delta e}\delta_e &= \hat{k}_p(\dot{h}_{ref} - \dot{h}) + \hat{k}_i\chi - \hat{k}_\theta\theta - \hat{k}_q q \\ &\quad + \hat{k}_f\dot{h}_{ref} + \hat{k}_v\ddot{h}_{ref} + \hat{k}_a\dddot{h}_{ref} + \hat{k}_d\ddot{\ddot{h}}_{ref}\end{aligned} \tag{42}$$

where $\hat{k}_p, \hat{k}_i, \hat{k}_\theta, \hat{k}_q, \hat{k}_f, \hat{k}_v, \hat{k}_a$, and $\hat{k}_d$ are the estimates of $k_p, k_i, k_\theta, k_q, k_f, k_v, k_a$, and k_d, respectively. To derive the parameter adaptation rules, we choose a Lyapunov function candidate

$$\begin{aligned}V_4 &= (1/2)(\lambda\chi_1^2 + z_1^2 + z_2^2 + z_3^2) + (1/2)(\tilde{k}_p^2/r_p + \tilde{k}_i^2/r \\ &\quad + \tilde{k}_\theta^2/r_\theta + \tilde{k}_q^2/r_q + \tilde{k}_f^2/r_f + \tilde{k}_v^2/r_v + \tilde{k}_a^2/r_a + \tilde{k}_d^2/r_d)\end{aligned} \tag{43}$$

where the parameter estimation errors are defined as

$$\begin{aligned}&\tilde{k}_p = k_p - \hat{k}_p, \ \tilde{k}_i = k_i - \hat{k}_i, \ \tilde{k}_\theta = k_\theta - \hat{k}_\theta, \ \tilde{k}_q = k_q - \hat{k}_q \\ &\tilde{k}_f = k_f - \hat{k}_f, \ \tilde{k}_v = k_v - \hat{k}_v, \ \tilde{k}_a = k_a - \hat{k}_a, \ \tilde{k}_d = k_d - \hat{k}_d\end{aligned} \tag{44}$$

The time derivative of V_4 along the trajectories of the system is computed by

$$\begin{aligned}\dot{V}_4 &= \lambda\chi_1 z_1 + z_1\dot{z}_1 + z_2\dot{z}_2 + z_3\dot{z}_3 \\ &\quad + \tilde{k}_p\dot{\tilde{k}}_p/r_p + \tilde{k}_i\dot{\tilde{k}}_i/r_i + \tilde{k}_\theta\dot{\tilde{k}}_\theta/r_\theta + \tilde{k}_q\dot{\tilde{k}}_q/r_q \\ &\quad + \tilde{k}_f\dot{\tilde{k}}_f/r_f + \tilde{k}_v\dot{\tilde{k}}_v/r_v + \tilde{k}_a\dot{\tilde{k}}_a/r_a + \tilde{k}_d\dot{\tilde{k}}_d/r_d\end{aligned} \tag{45}$$

We can recalculate the time derivative of V_4 in (45) as

$$\dot{V}_4 = -(K_1 - Z_\alpha)z_1^2 - (K_2 - K_1)z_2^2 - (K_3 - C_{33})z_3^2$$

$$+\tilde{k}_p[z_3(\dot{h}_{ref}-\dot{h})-\dot{\hat{k}}_p/r_p]+\tilde{k}_i[z_3\chi_1-\dot{\hat{k}}_i/r_i]$$
$$+\tilde{k}_\theta[z_3\theta-\dot{\hat{k}}_\theta/r_\theta]+\tilde{k}_q[z_3 q-\dot{\hat{k}}_q/r_q] \quad (46)$$
$$+\tilde{k}_f[z_3\dot{h}_{ref}-\dot{\hat{k}}_f/r_f]+\tilde{k}_v[z_3\ddot{h}_{ref}-\dot{\hat{k}}_v/r_v]$$
$$+\tilde{k}_a[z_3\dddot{h}_{ref}-\dot{\hat{k}}_a/r_a]+\tilde{k}_d[z_3\ddddot{h}_{ref}-\dot{\hat{k}}_d/r_d]$$

If the parameter adaptation rules are selected as

$$\dot{\hat{k}}_p=r_p z_3(\dot{h}_{ref}-\dot{h}),\ \dot{\hat{k}}_i=r_i z_3\chi_1,\ \dot{\hat{k}}_\theta=r_\theta z_3\theta,\ \dot{\hat{k}}_q=r_q z_3 q \quad (47)$$
$$\dot{\hat{k}}_f=r_f z_3\dot{h}_{ref},\ \dot{\hat{k}}_v=r_v z_3\ddot{h}_{ref},\ \dot{\hat{k}}_a=r_a z_3\dddot{h}_{ref},\ \dot{\hat{k}}_d=r_d z_3\ddddot{h}_{ref}$$

which leads to obtain the following time derivative of V_4

$$\dot{V}_4=-(K_1-Z_\alpha)z_1^2-(K_2-K_1)z_2^2-(K_3-C_{33})z_3^2 \quad (48)$$

$\dot{V}_4$ becomes negative semidefinite when conditions (47) are satisfied. By using Barbalat's lemma (Krstic, *et al.*, 1994), it shows that $z_1\to 0$, $z_2\to 0$, and $z_3\to 0$ as $t\to\infty$.

5. COMPUTER SIMULATIONS

Although derived based on the linearized model (1), the proposed adaptive auto-landing controller must be shown effective and useful on the nonlinear model of the aircraft. Hence, this section is devoted to conducting several computer simulations using the aircraft nonlinear 6-DOF equations of motion, in order to examine the efficacy of the proposed controller of (42) and (47) from wing-level flight to flare. The simulations also investigated the performance of the proposed auto-landing controller without and with wind turbulence from glide-slope to flare maneuver. In doing these simulations, the localizer control for the lateral/directional axes was synthesized for maintaining a constant heading angle instead of course deviation tracking. To show the effectiveness of the proposed controller, all simulations following the auto-landing commands should meet the following conditions and scenarios: 1) the time constant (τ) and the flare initiation height (h_0) must be pre-determined, and the values of τ and h_0 are 2.98 sec and 18.47 ft, respectively; 2) the UAV is trimmed at speed of 70 knots/altitude of 200 ft and the initial distance is 4000 ft away from touchdown point; 3) the glide-slope mode is engaged from 3816 ft (H_0/tan(γ_{GS})) away from touchdown point depending on the initial altitude (H_0=200ft) and the desired glide-slope angle; 4) the elevator actuator is modeled as a first-order system model with a time constant of 0.1 sec. with a rate limit of 60 deg/sec, and the throttle servo is ignored; 5) the parameters K_1, K_2, and K_3 are easily obtained from (42), and K_1=1.5, K_2=2.3, K_3=8.0, K_4=1.5e-4, K_I=25, w_T=0.1 and adjusted factor k=20 are selected in the simulations with $\gamma_{j(j=p,I,\theta,q,f,v,a,d)}$=1e-6.

For saving space, the time histories of auto-landing trajectories without wind turbulence are omitted here. The simulation results without wind turbulence reveal that there exists a smooth transition from glide-slope to flare mode, and the glidepath and altitude are shown consistent with their desired values. Besides, the proposed controller has shown the desired touchdown performance. We only show the dynamic performance with wind turbulence (u_0=20 ft/sec) and wind shear (w_0=20 ft/sec). To start the simulations with wind turbulence, it is assumed that the winds were activated at steady-state descending at t = 10 sec. Fig. 2 shows the time histories of angle of attack, pitch angle, flight-path angle, vertical speed, altitude, velocity, throttle, and elevator during the landing phases. The results in Fig. 2 indicate that the speed PI controller may not maintain the constant thrust and speed immediately. This is because the velocity, the pitch angle, and the altitude of the light-weight UAV are easily affected by the phugoid mode in a large wind. Even so, the vertical speed and pitch angle at touchdown point still lie within the auto-landing specifications. The results in Fig. 3 clearly show that the proposed controller tracks the prespecified altitude trajectory from glide-slope to flare maneuver, and gives the satisfactory touchdown distance in the presence of wind turbulence. Fig. 4 shows time responses with the vertical wind shear. It is observed that the adaptive controller is trying to catch up the desired altitude under the simulated microburst environment. Fig. 5 shows that the controller performs well in the altitude trajectory under the wind shear. Through these simulation results, the adaptive backstepping controller has been proven capable of effectively guiding the light-weight UAV along the glidepath commands under the wind turbulence and wind shear.

6. CONCLUSIONS

In this paper, an auto-landing control law for an unmanned aerial vehicle has been established using adaptive backstepping with a forward speed PI controller, and a flight path command generator has been derived to provide an appropriate trajectory. The proposed adaptive control law has been designed to accomplish longitudinal auto-landing for the two maneuvers (glide-slope and flare) without any additional input. In addition, such an auto-landing controller can be shown much simpler, and easier to construct and realize than conventional control methods. More importantly, the kind of adaptive controller with parameter adaptation rules has brought about precision in the flight path following such that a successful auto-landing can be performed, in which the desired altitude and flight path responses are achieved by indirect altitude control even in the presence of the wind turbulence and microburst.

REFERENCES

Ebrahimi, Y.S. and E.E. Coleman (2001). Design of localizer capture and track using classical control techniques. *Proceedings of the IEEE Control System Magazine,* **10**, pp. 5-12.

Liao, F., J. L. Wang, E. K. Poh, and D. Li (2005). Fault-tolerant robust automatic landing control design. *Journal of Guidance, Control, and Dynamics,* **28**, pp. 854-871.

Ha, C. and J. Kim (2005). Automatic landing under wind shear turbulence in adaptive gain scheduled PID control optimized in genetic algorithm. *AIAA Guidance, Navigation, and Control Conference and Exhibit,* San Francisco, California, AIAA-2005-6346.

Harkegard, O. and G.T. Torkel (2000). A backstepping design for flight-path angle control. *Proceedings of the IEEE Conference on Decision and Control*, **4**, pp. 3570-3575.

Iiguni, J and H. Akiyoshi (1998). An intelligent landing system based on a human skill model. *IEEE Transaction on Aerospace and Electronic Systems*, **34**, pp. 877-882.

Izadi, H, M. Pakmehr and N. Sadati (2003). Optimal neuro-controller in longitudinal auto-landing of a commercial jet

transport. *Proceedings of IEEE Conference on Control Applications,* **1**, pp. 492-497.

Jorgensen, C.C. and C. Schley (1990). Neural network baseline problem for control of aircraft flare and touchdown. *Neural Networks for Control,* Cambridge, MA: MIT Press.

Ju, H.S. and C.C. Tsai (2007). Longitudinal axis flight control law design by adaptive backstepping. *IEEE Transactions on Aerospace and Electronic Systems*, **43**, pp. 311-329.

Ju, H.S., C.C. Tsai and C.T. Lee (2005). Flight path control design for glide-slope tracking by backstepping. *Proceedings of the 2005 IEEE International Conference on Mechatronics*, pp. 887-892.

Juang, J.G. and K.C. Cheng (2001). Wind disturbances encountered during controlled landings using neural network approaches. *Proceedings of the IEEE International Conference on Control Applications*, pp. 835-840.

Kaminer, I., and P.P. Khargonekar (1990). Design of the flare control law for longitudinal autopilot using H_∞ synthesis. *Proceedings of the IEEE Conference on Decision and Control,* **Vol. 6**, pp. 2981-2986.

Kim, D., Y. Choi and J. Suk (2005). A glidepath tracking algorithm for autolanding of a UAV. *Infotech@Aerospace,* Arlington, Virginia, AIAA-2005-6979.

Krstic, M., I. Kanellakopoulos and P. Kokotovic (1995). *Nonlinear and Adaptive Control Design*. John Wiley & Sons, Inc., New York.

Lee, T. and Y. Kim (2001). Nonlinear adaptive flight control using backstepping and neural networks controller. *AIAA Journal of Guidance, Control, and Dynamics*, **24**, pp. 675-682.

Li, Y., N. Sundararajan, P. Saratchandran and Z. Wang (2004). Robust neuro-H^∞ controller design for aircraft auto-landing. *IEEE Transactions on Aerospace and Electronic Systems*, **40**, pp. 158-167.

Nho, K. and R.K. Agarwal (2000). Automatic landing system design using fuzzy logic. *Journal of Guidance, Control, and Dynamics,* **23**, pp. 298-304.

Niewoehner, R.J. and I.I. Kaminer (1996). Design of an autoland controller for an F-14 aircraft using H_∞ synthesis. *AIAA Journal of Guidance, Control, and Dynamics,* **19**, pp. 656-663.

Ochi, Y and K. Kanai (1999). Automatic approach and landing for propulsion controlled aircraft by H_∞ control. *Proceedings of the IEEE Conference on Control Applications,* **2,** pp. 997-1002.

Saini, G and S.N. Balakrishnan (1997). Adaptive critic based neurocontroller for autolanding of aircrafts. *Proceedings of the 1997 American Control Conference,* **2**, pp. 1081-1085.

Sharma, M. and D.G. Ward (2002). Flight-path angle control via neuro-adaptive backstepping. *AIAA Journal of Guidance, Control, and Dynamics*, AIAA2002-4451.

Shue, S.P. and R.K. Agarwal (1999). Design of automatic landing systems using mixed H_2/H_∞ Control. *AIAA Journal of Guidance, Control, and Dynamics,* **22**, pp. 103-114.

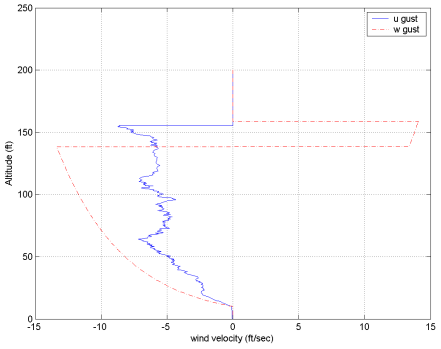

Fig. 1. Wind profile: wind turbulence and wind shear

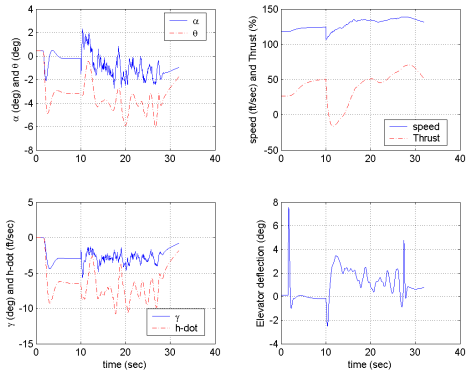

Fig. 2. Auto-landing time responses with wind turbulence.

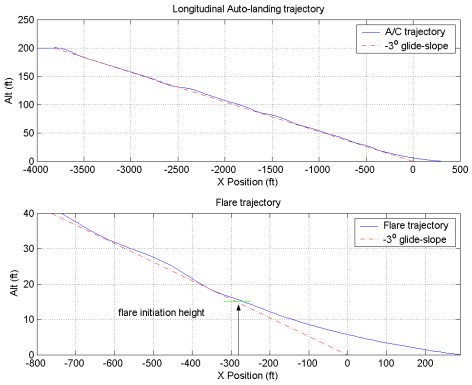

Fig. 3. The altitude trajectory with wind turbulence. Top: altitude response. Bottom: magnified view.

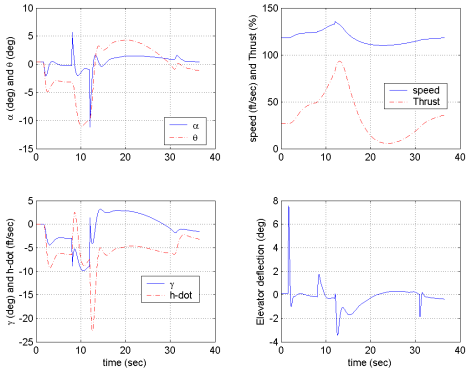

Fig. 4. Auto-landing time responses with wind shear.

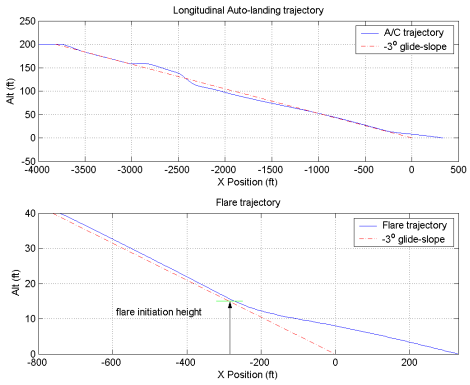

Fig. 5. The altitude trajectory with wind shear. Top: altitude response. Bottom: magnified view.